Research Article **Open Access**

Proline-rich peptide-linked albumin particles in an experimental oxidative brain damage model

Kristine Edgar Danielyan[1,*], Nazeli Zaqaryan [1], Rita Khallouf [1], Maria Kojoyan[1], Kristine Tspnetsyan[1], Arpi Manukyan[1], Astghik Tsokolakyan [2], Mkrtich Alexan Yeranosyan [2], Samvel G. Chailyan [1]

A. B. Nalbandyan Institute of Chemical-Physics, National Academy of Sciences, Republic of Armenia, Yerevan 0014, Armenia; H. Buniatian Institute of Biochemistry, National Academy of Sciences, Republic of Armenia, Yerevan 0014, Armenia.

Corresponding author: Kristine Danielyan, PhD, H. Buniatian Institute of Biochemistry, 5/1 building, Paruyr Sevak Street, Yerevan 0014, Armenia.

Submission Date: September 24th, 2025; **Acceptance Date:** November 27th, 2025; **Publication Date:** December 1st, 2025

Please cite this article as: Danielyan K. E., Zaqaryan N., Khallouf R., Kojoyan M., Tspnetsyan K., Manukyan A., Tsokolakyan A., Yeranosyan M. A., Chailyan S. G. Proline-rich peptide-linked albumin particles in an experimental oxidative brain damage model. *Bioactive Compounds in Health and Disease* 2025; 8(12): 527 – 544. DOI: https://doi.org/10.31989/bchd.v8i12.1835

Abstract

Background: The leading contributors to death and disability are cardiovascular diseases (CVDs) and stroke. PRP-1 (Proline Rich Peptide) is a peptideisolated from the bovine hypothalamus and identified in the human brain. It was shown that this peptide may have antioxidant and neuroprotective properties. However, the circulation time of peptides in the bloodstream is limited; therefore, coupling PRP-1 with albumin nanoparticles might prolong its stability and bioavailability. The purpose of the study was to evaluate PRP-1 conjugated with albumin nanoparticles in an experimental brain injury model induced by hydrogen peroxide.

Methods: We used Transmission Electron Microscopy (TEM; Philips CM10) and Dynamic Light Scattering (DLS) to evaluate particle size and zeta potential. The brain injury model was created using hydrogen peroxide as a source of free radicals, which induced disruption of the blood–brain barrier (BBB). BBB disruption was quantified by measuring Evans Blue dye accumulation in the brain parenchyma.

Results: Through sedimentation and filtration procedures, we obtained stable nanoparticles (NPs). PRP-1–coupled NPs degraded more slowly in the presence of trypsin than control NPs. Furthermore, PRP-1/NPs partially prevented BBB disruption in the experimental model.

Conclusion: PRP-1/albumin NPs protected the BBB under experimental brain injury conditions.

Keywords: PRP-1, neurohormone, experimental stroke, albumin, nanoparticles, blood–brain barrier

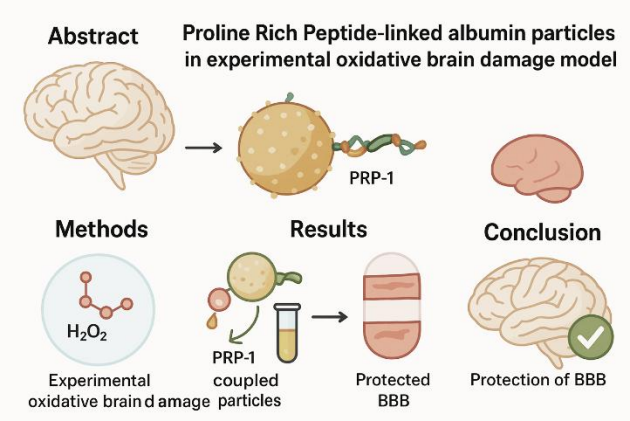

Graphical Abstract: Proline-rich peptide-linked albumin particles in an experimental oxidative brain damage model.

INTRODUCTION

Galoyan A.A. and co-authors were the first to discover novel neurohormone-like peptides isolated from neurosecretory granules of the human and bovine neurohypophysis [1-2]. Most of these peptides are rich in the structurally rare amino acid proline, a feature also well documented in peptides synthesized by salivary glands [3]. The newly identified neuropeptide family, designated by Galoyan A.A. and colleagues, includes members PRP-1 through PRP-4, consisting of 15, 14, 13, and 10 amino acids, respectively [4-5].

According to mass spectrometry, the molecular mass of human PRP-5 has been determined as 1560.5 Da [4].

Human PRPs differ from their bovine analogs by three amino acids [4]. Localization of bovine PRP was first revealed by immunohistochemistry: PRP was detected in magnocellular neurons of the nucleus supraopticus (NSO) and in parvocellular neurons of the rostral and medial subdivisions of the nucleus paraventricularis (NPV) in the rat brain. Immunoreactivity was stronger in the NSO than in the NPV [1-2].

A series of publications by Galoyan A.A. describes the mechanisms of PRP generation and transport to target organs. The authors suggest that these peptides arise from proteolytic cleavage of the C-terminal portion of the neurophysin–vasopressin-associated glycoprotein and may be co-transported with vasopressin and oxytocin from the hypothalamus to the neurohypophysis via axonal transport [4]. The physiological effects of PRPs are wide-ranging, likely due to their neurohormonal nature [1-2,4]. Their biological effects depend on dose, timing, organismal state, and route of administration [4]

It is well established that the half-life of peptides in the bloodstream is short due to proteolysis [6]. To address this limitation, we aimed to prolong with albumin nanoparticles. A single treatment costs. Therefore, we propose binding PRP-1 with albumin

nanoparticles both to extend its circulation time and to test whether a low dose of PRP-1/albumin nanoparticles can protect the rat brain in experimental stroke settings.

MATERIALS AND METHODS

Purification of Xanthine Oxidoreductase: Fresh bovine milk (400 mL) without preservatives was chilled at 4 °C overnight [7]. The milk was churned at speed using a blender for 30 minutes at room temperature, during which the temperature rose from 4 °C to 45 °C. After cooling the churned milk back to ~4 °C, the churning process was repeated. The resulting mixture was filtered through six layers of cheesecloth.

The opalescent filtrate (300 mL) was brought to 50% ammonium sulfate saturation by adding solid ammonium sulfate. The suspension was centrifuged at 8,000 × g for 15 minutes, and the precipitate was discarded. The supernatant (360 mL) was then centrifuged at 10,000 × g for 30 minutes. The final supernatant was dissolved in 10 mM Tris–HCl buffer (pH 7.6) containing mM EDTA.

This solution was dialyzed against 0.1 M PBS containing 100 mM EDTA. Protein purification was performed by gel filtration chromatography (Figure 5A) using Sephadex G-200 (Sigma-Aldrich-Merck, USA). A weak 0.01 M NaCl solution was used as the eluent to minimize nonspecific protein binding to the gel.

For final purification, semi-affinity chromatography on DEAE-Sephacel (Sigma-Aldrich-Merck, USA) was performed. The sample was loaded onto a pre-equilibrated DEAE-Sephacel column (15 × 2 cm) and washed with the same buffer until the absorbance at 280 nm decreased to ≤ 0.030.

XOR (Xanthine Oxidoreductase) samples were concentrated using a rotary evaporator (200 rpm, 50 °C). Based on previous work, these conditions do not affect XOR activity [8].

RP-HPLC Analysis: The purity of XOR extracted from milk was assessed using reverse-phase high-performance liquid chromatography (RP-HPLC) (Figure 5B). A Shimadzu LC-20 chromatograph equipped with an SM 5000 UV-Vis detector and C18 reverse-phase columns (Avex, Waters, and Symmetry) was used. Elution was carried out under isocratic conditions at a flow rate of 2 mL/min with degassed water as the mobile phase. Absorbance was monitored at 280 nm, and elution was completed within 10 minutes.

XOR Activity Measurement: Enzyme activity was determined by measuring uric acid content according to the method of Litwack, Bothwell et al [9].

Xanthine, PRP-1, and allopurinol (0.4 µg per 1 mL) were incubated with the purified enzyme (0,088 mg/mL) for 40 minutes at 36.6 °C.

Absorbance was recorded at 660 nm using a Cary 60 spectrophotometer (Agilent, USA). Protein concentration was determined by the Lowry method [10]. Specific enzymatic activity was calculated as:

$$A\,(\mu\mathrm{M/min/mg}) = \frac{P\,(\mu\mathrm{M})}{t\,(\mathrm{min}) \times \mathrm{protein}\,(\mathrm{mg})}$$

Unless otherwise specified.

Docking Analyses: The amino acid sequence of Proline-Rich Peptide (PRP) was obtained from UniProt. The peptide structure was built in UCSF Chimera, followed by the addition of hydrogen atoms and the assignment of Gasteiger charges. Conformations were refined using the Rotamers tool to optimize side-chain geometry. The ligand structure was further refined in PyMOL before docking with AutoDock Vina.

The structure of XOR was retrieved from the RCSB Protein Data Bank (PDB) and prepared using MGL AutoDock Tools 1.5.6. Hydrogen atoms were added, polar hydrogens were optimized, and Kollman charges were assigned. The active site was defined as a 60 Å × 60

Å × 60 Å grid box, centered at (x = 114.084, y = 20.299, z = 112.253). The prepared protein was saved in PDBQT format for docking.

Docking was performed to evaluate potential interactions of PRP with the XOR active site. Binding affinities were calculated using AutoDock Vina's scoring function. Favorable ligand–target interactions were visualized and analyzed with Discovery Studio Visualizer 2021.

Generation of Albumin Particles: Five hundred microliters of 20% bovine albumin (Arpimed, Armenia) were diluted in 1 mL of water. Subsequently, 10 µL of 40% glutaraldehyde (Medisar, Armenia) and 1 mL of ethanol were added. In selected experimental groups, PRP-1 was introduced at a final concentration of 165 µg/mL. The mixture was incubated for 24 hours and then centrifuged at 14,000 × g for 30 minutes. After centrifugation, the supernatant was removed, and the particles were purified by dialysis against 0.1 M PBS to eliminate residual glutaraldehyde [10].

For the in vivo experiments, we aimed to inject no more than 100 µL of any solution to avoid dramatically altering blood composition. Based on previous experimental results on the effective PRP-1 dosage [11], we prepared PRP-1/NPs at a concentration of 165 µg/mL. Consequently, each animal weighing approximately 200 g received approximately 16.5 µg of PRP-1 included in the composition of NPs (Nanoparticles).

Measurement of ζ-Potential and Hydrodynamic Diameter: Particle hydrodynamic diameters were measured using dynamic light scattering (DLS) on a Litesizer™ 500 instrument (Anton Paar, Graz, Austria).

Measurements were performed at 25 °C under automatically optimized settings for latex particles. The ζ-potential was assessed using an Omega Z cuvette (Anton Paar) with a 40 mW laser operating at 658 nm. Each measurement consisted of 40 runs to ensure accuracy and reproducibility [12].

Transmission Electron Microscopy: Albumin-based microcarriers and nanoparticles were characterized using a Philips CM10 transmission electron microscope (TEM). A droplet of the sample was deposited onto 200-mesh copper grids coated with polyvinyl formal and allowed to absorb for 2 minutes. Grids were gently rinsed with Milli-Q water and stained with 2% uranyl acetate [13].

Excess stain was removed using filter paper, and the grids were air-dried. Imaging was performed at 25,000× magnification.

Vertebrate Animals: All animal experiments were conducted in compliance with the Institutional Animal Care and Use Committee (IACUC) guidelines and the ethical standards of the Armenian Ethical Committee of the H. Buniatian Institute of Biochemistry, National Academy of Sciences of the Republic of Armenia. Procedures for anesthesia, euthanasia, surgery, and blood collection adhered to approved protocols.

Adult Albino laboratory rats (males, ~200 g) were anesthetized via intraperitoneal injection of pentobarbital sodium (2 mg per 100 mg body weight). Complete anesthesia was achieved within five minutes and confirmed by the absence of reflexive movement in response to leg pinching. Supplemental doses were administered as needed.

During surgery, cranial and rectal temperatures were continuously monitored to ensure physiological stability. Seven days post-procedure, animals were deeply anesthetized and euthanized via cervical dislocation. Postoperative observations and interventions were carefully recorded.

All rats received perioperative analgesia- tramadol (10–20 mg/kg SC 30 minutes before surgery and every 8 hours for 48 hours post-op [14], plus meloxicam 1 mg/kg

SC once daily for 48–72 hours [15]. Animals were monitored at least twice daily for pain, surgical complications, and recovery; rescue analgesia (additional buprenorphine 5 mg/kg SC) was given when pain signs were observed. care and use committee.

Experimental Brain Injury Model in Rats: Brain injury was induced by stereotaxic injection of 5 µL of 3% hydrogen peroxide into the brain parenchyma following a limited craniotomy. Hydrogen peroxide was injected stereotaxically at AP +3.0 mm, ML ±2.0 mm relative to bregma, and DV −2.0 mm from the skull surface (dura; injection depth). Coordinates were determined based on the skull flat (bregma–lambda plane level) and adjusted according to the Paxinos & Watson [16] coordinates. A stereotaxic frame designed for rats ensured accurate delivery [17]. A 27-gauge stainless steel cannula with a 30° bevel was used. After injection, the needle was left in place for several minutes before being slowly withdrawn. The burr hole was sealed with bone wax, and the scalp was sutured. Postoperatively, rats were returned to cages with unrestricted access to food and water [18]

Neurological Deficit Assessment: A standardized, quantitative neurobehavioral battery was administered to assess sensorimotor function 2 hours after the brain-damage procedure, as well as at 6, 24, 48, and 72 hours. The tests are sensitive and detect even mild sensorimotor dysfunction in investigations [18]. The neurobehavioral assessment included the postural reflex and limb placing tests, as previously described [19-20]. Neurological function was scored on a 0–12 scale (0 = normal, 12 = maximal deficit). All tests were conducted by a researcher blinded to treatment allocation.

Particle Circulation Assessment: Intact and brain-injured rats received intravenous injections via the jugular vein containing 1.08–1.10 × 10^8 albumin or albumin/PRP-1 particles. One hour post-injection, blood samples were collected into heparinized tubes and centrifuged at 1,000 × g for 10 minutes. Plasma was isolated, and particle concentrations were determined using a hemocytometer. Images of sample fields were captured and analyzed with Pixcavator 5 software (Peter Saveliev, Marshall University, WV, USA) using a trinocular phase-contrast microscope (Boeco GmbH) with a 100× objective.

Evans Blue Extraction and Blood–Brain Barrier Assessment: Blood–brain barrier (BBB) integrity was evaluated by quantifying Evans Blue (EB) dye accumulation. A 4% EB solution in saline (4 mL/kg) was injected intravenously via the jugular vein one hour before euthanasia. Under anesthesia, thoracotomy was performed, and animals were perfused with 3 L of 0.1 M PBS via the left ventricle to clear intravascular dye [18].

After decapitation, brains were removed, frozen, and sectioned into 1 mm coronal slices from bregma +2.7 mm to −0.3 mm. Sections were divided into hemispheres and dissected for EB quantification [21].

Statistical Analysis: Data are expressed as mean ± SEM. Statistical significance between groups was analyzed using one-way analysis of variance (ANOVA), Student's t-test, and two-way repeated-measures ANOVA. Differences with $p < 0.05$ were considered statistically significant.

RESULTS

Docking analyses

Xanthine: The O^2 atom of the purine ring formed hydrogen bonds with Gln767 and Gly799. The N^3 atom formed a hydrogen bond with Thr1077. Van der Waals interactions were observed with Phe798, Arg912, Gln1194, Gln1040, Ser1082, and Ala1078. Ser1080 established an amide–π stacked interaction, while Gly1260 and the O^6 atom formed a carbon–hydrogen bond (Figure 1A).

Allopurinol: Docking analysis revealed predominant hydrogen bond formation between XOR and the purine ring of allopurinol: the N^9 atom of purine ring interacted with Gln1194, the N^2 atom - with Met1037, and the O^6 atom - with Gly797/798. Additional interactions included a π–carbon bond with Arg912 and a π–alkyl bond with Cys150 (Figure 1B).

PRP-1. PRP-1 interacted with XOR mainly via hydrogen bonds with Pro753, Gly820, Lys33, Arg32, Leu34, Arg37, and Gly588. Alkyl and π–π-alkylπ-alkylπ-alkyl interactions were observed with Lys754, Pro597, Ile596, Leu36, Val10, and Lys13. His821 contributed a π–π T-shaped interaction; Gly35 formed a carbon–hydrogen bond; Arg598 and Glu89 participated in attractive charge interactions (Figure 1C).

Substrates, inhibitors, and PRP-1 interacted with XOR through different dominant mechanisms: xanthine via van der Waals forces, allopurinol via hydrogen bonds, and PRP-1 via alkyl/π–alkyl interactions. Binding affinity was highest for PRP-1 (−9.38 kcal/mol), likely due to the formation of both alkyl/π–alkyl interactions and seven hydrogen bonds. Xanthine (−6.33 kcal/mol) exhibited stronger binding than allopurinol (−5.94 kcal/mol) (Table 1, Figure 1).

Table 1. Comparison of the effectiveness of the binding of XOR with novel ligand, substrate, and classical inhibitor.

Compounds	Binding affinity (kcal/mol)	RMSD
PRP-1	-9.38	136.7
Allopurinol	-5.94	158.06
Xanthine	-6.33	30.498

Animal XORs are homodimeric enzymes with an approximate molecular mass of 300 kDa [22].

Each subunit comprises a single polypeptide chain of approximately 1,330 amino acids and incorporates multiple cofactors: one molybdopterin cofactor (Mo-pt), two distinct [2Fe–2S] clusters, and one flavin adenine dinucleotide (FAD) cofactor [22]. These cofactors are spatially distributed across three structural domains: the C-terminal domain (~85 kDa), the N-terminal domain (~20 kDa), and an intermediate domain (~40 kDa) [22].

Xanthine oxidation takes place at the molybdenum center, and the electrons produced during this reaction are rapidly transferred to FAD via the Fe–SI and Fe–SII clusters [23].

The final step, reoxidation of the reduced enzyme by an electron acceptor—either NAD^+ or molecular oxygen—is facilitated by the FAD cofactor [24-25].

Each XOR monomer can be divided into three subdomains. The small N-terminal domain (residues 3–164) contains both iron–sulfur centers and is connected to the FAD-binding domain (residues 192–527) via a flexible, partially disordered linker region (residues 165–192) [24-25]. Our molecular docking analyses suggest that PRP-1 partially interacts with residues within these domains.

The third and largest domain (residues 590–1315) encompasses the molybdopterin cofactor and lies near the interface between the iron–sulfur and FAD-binding regions [24-25]. Docking studies indicate that PRP-1 shows stronger and more consistent interactions within this domain, similar to inhibitors, such as xanthine and allopurinol. These in silico findings were supported by in vitro experiments, observed, which showed significant inhibition of XOR activity by PRP-1, corroborating the docking results.

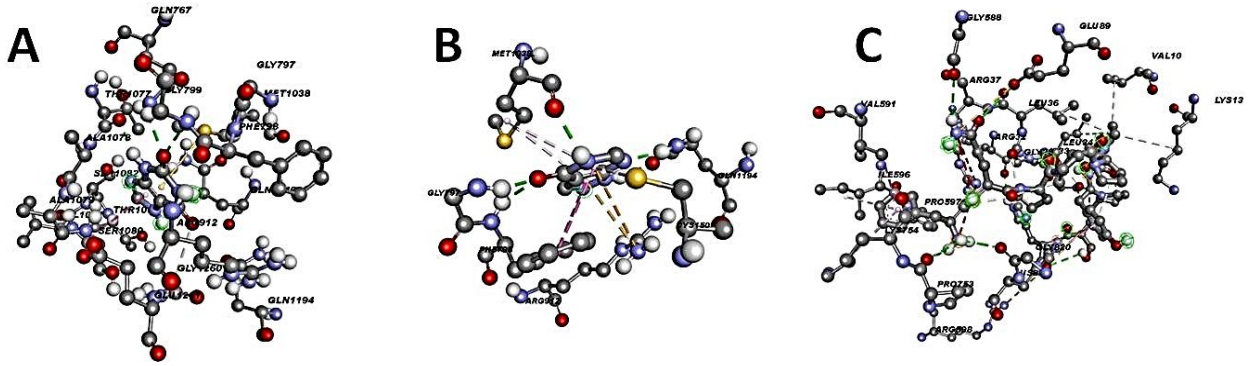

Figure 1. Docking analyses of XOR with substrate, inhibitor, and novel ligand. A. Interaction of XOR with xanthine. B. Docking analyses of allopurinol with XOR. C. Interaction of XOR with PRP-1.

Measurement of the Generated Particle Sizes; After analyzing the series of samples, we concluded that the particle sizes ranged from 100 nm to 2 microns. To obtain smaller particles for subsequent in vivo experiments (Figure 2), we techniques.

DLS showed an average hydrodynamic diameter of 38,11±0,78 after filtration, with a polydispersity index (PDI) of 28,53±0,08 for the albumin NPs group and 34,1±0,4 hydrodynamic diameter with a PDI of 28,06±0,51 for the PRP/NPs group.

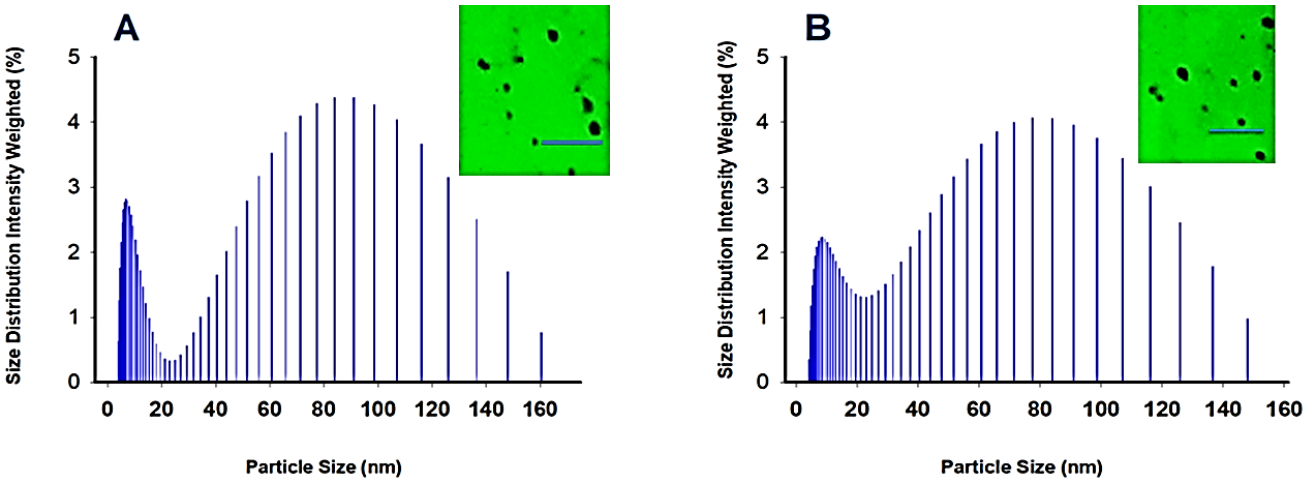

Figure 2. Determination of the size as well as the shape of the particles for further utility of them for in vivo and in vitro experiments. A.B. Inserts. The TEM image of particles produced from HSA and HAS/PRP-1 without the filtration step. It was applied at a 25000 times magnification. Philips CM-100 TM Electron Microscopy was used for the purpose mentioned above. **A.** Size-determined distribution of albumin particles. B. Size-determined distribution of albumin/PRP-1 particles. The line measure on the picture represents 10 microns.

Evaluation of Zeta Potential: As a measure of stability, we evaluated the ζ-potential of particles in two groups: one containing PRP-1 and the other composed solely of polymerized albumin. The ζ-potential values for these groups were −21.27 ± 3.83 mV and −23.07 ± 2.82 mV, respectively (Figure 3C', D'). Conductivity, the primary parameter used to assess particle charge, measured $0.389 \pm 5.01 \times 10^{-3}$ S/m for the albumin group and $0.450 \pm 5.03 \times 10^{-3}$ S/m for the PRP-1/albumin group ($p < 0.0001$) (Figure 3A). The difference in electrophoretic mobility between the two groups was minimal, with values of −1.97 ± 0.11 µm·cm/V·s and −1.60 ± 0.29 µm·cm/V·s for albumin and PRP-1/albumin, respectively (Figure 3B).

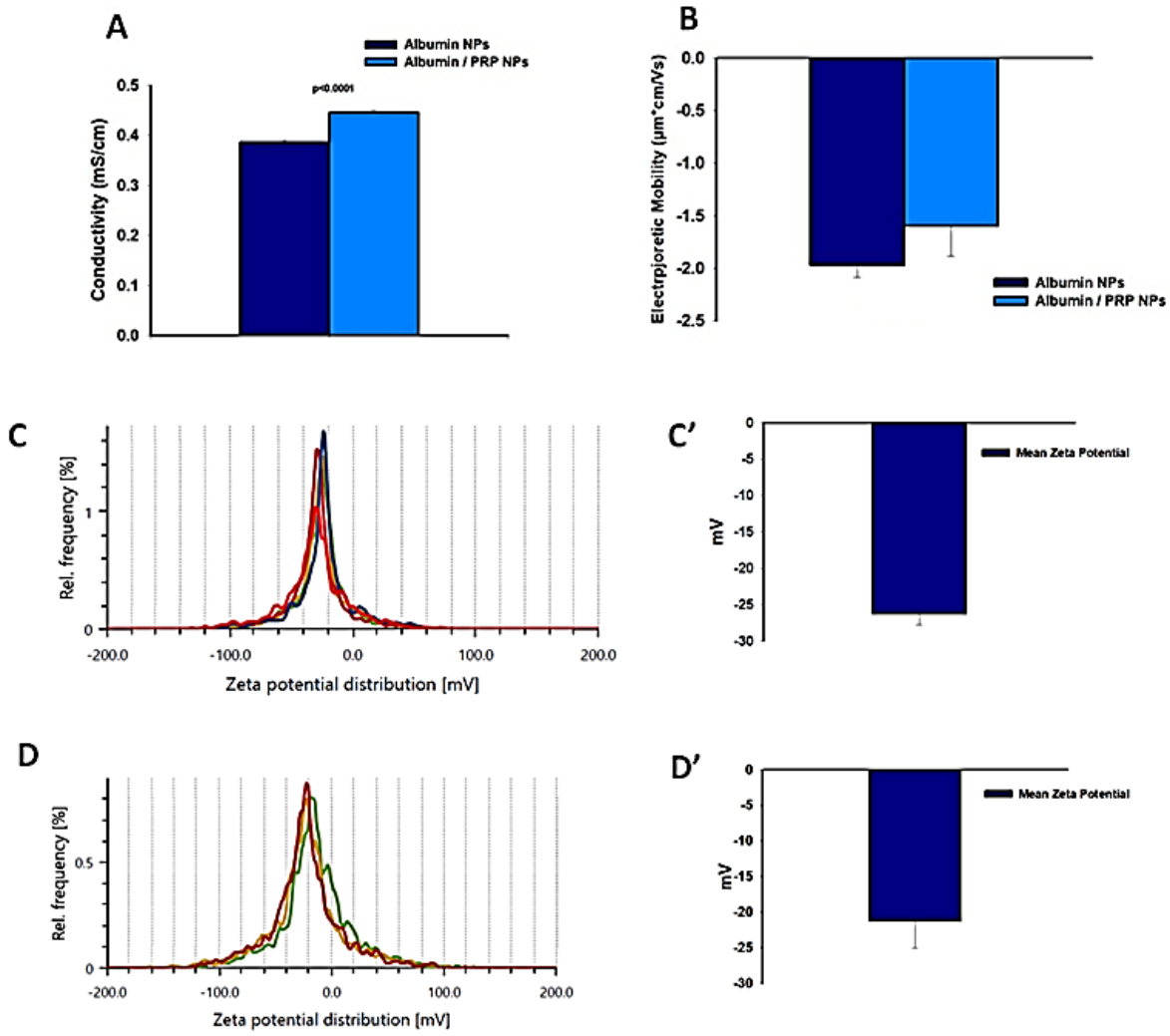

Figure 3. Evaluation of physical-chemical properties of NPs. **A.** Comparison of albumin vs albumin/PRP-1 particles' conductivity (t-test, p= 3.40E-06). **B.** Comparison of albumin vs albumin/PRP-1 particles' electrophoretic mobility (t-test, p= 0.035)**. C.** Zeta potential reading for albumin particles group (representation of the individual graphs for the entire group). **C'.** Mean Zeta potential value (±SEM) for particles in the albumin particle group. **D.** Zeta potential reading for albumin/PRP-1 particles group (representation of the individual graphs for the entire group)**. D'.** Mean Zeta potential value (±SEM) for albumin/PRP-1 particles group.

Coupling of the peptide with NPs: Figure 4 illustrates the coupling ability of PRP-1 with NPs through chemical bonding via GA. The binding efficiency was assessed by measuring the protein content in the supernatant after centrifugation, since peptide-bound particles were pelleted while unbound peptide remained in the supernatant. The first column of the graph represents the initial peptide amount added equally to both sample types—those with and without particles. The free peptide concentration in the samples was 54.41 ± 4.00 mg, but after the addition of GA and NPs, the protein content in the supernatant decreased to 19.0 ± 3.98 mg.

The coupling efficiency, calculated from the loss of free peptide in the supernatant, was 65.1±7.3 %, indicating that approximately two-thirds of the added PRP-1 became covalently associated with the GA-activated NPs.

Proteolysis of PRP-1 vs PRP-1/ NPs: In this experiment, potassium sodium tartrate was used as a general trypsin

inhibitor together with PRP-1. The results of the in vitro proteolysis assay are shown in Figure 4B.

During the first 24 hours of incubation, PRP conjugation noticeably slowed down the proteolytic degradation of nanoparticles. The supernatant protein concentration for PRP/NPs reached only 0.77 ± 0.012 mg/mL, compared to 0.83 ± 0.04 mg/mL for NPs, indicating a modest but measurable delay in trypsin lysis. However, between 24 and 48 hours, the degradation rate increased and by 48 hours both formulations showed comparable high protein release. Specifically, for NPs group, protein content increased from 0.83 ± 0.04 mg/mL to 1.87 ± 0.07 mg/mL (absolute increase 1.04 ± 0.08 mg/mL, mean release rate 0.043 ± 0.003 $mg \cdot mL^{-1} \cdot h^{-1}$, ≈2.25-fold rise). For PRP/NPs, the increase was from 0.77 ± 0.012 mg/mL to 1.80 ± 0.09 mg/mL (absolute increase 1.03 ± 0.09 mg/mL, mean rate 0.043 ± 0.004 $mg \cdot mL^{-1} \cdot h^{-1}$, ≈2.3-fold rise). Thus, PRP coating provided transient protection against enzymatic degradation during the initial 24 hours, but the long-term degradation profile of PRP/NPS is similar to NPs by 48 hours.

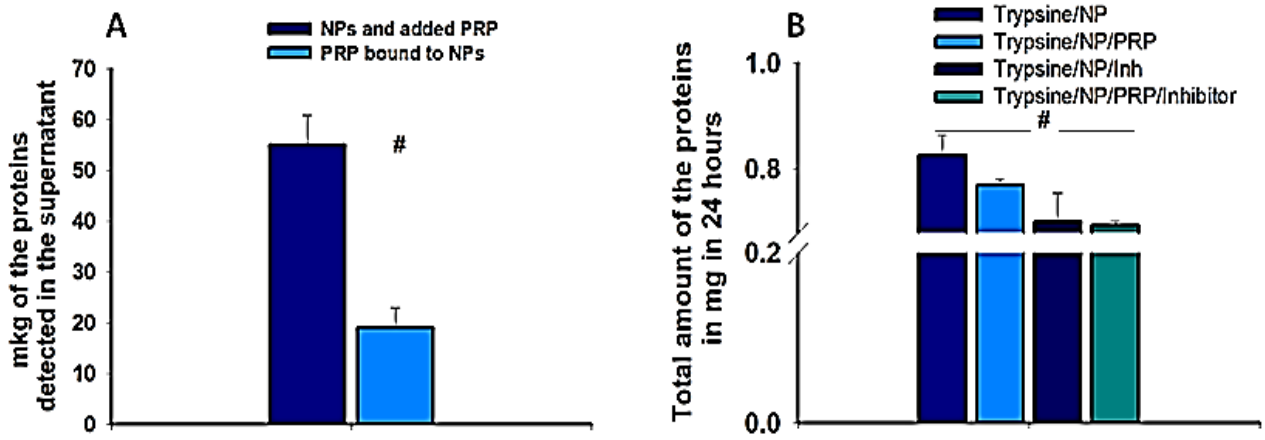

Figure 4. A. Binding of the PRP-1 with the albumin particles. The binding process was determined by the utility of the Lowry method for the measurement of proteins. A Cary 60 spectrophotometer (Agilent, USA) was used. The Student's t-test was applied to determine the significance of the results. The results were statistically significant, with $p<0.05$ (n=10 ~~per group~~). **B.** The simultaneous impact of PRP-1, along with the general protease inhibitor KNaC4H4O6*4H2O, is suppressing the trypsinolyses during 24 hours of incubation.

Normality and homogeneity of variances were assessed to analysis (n=5). The data passed the normality test (Shapiro–Wilk, P = 0.277) but failed the equal-variance test ($P < 0.05$). Therefore, a nonparametric Kruskal–Wallis one-way analysis of variance on ranks was performed. The study revealed a statistically significant difference among groups ($H(3) = 6.67$, P = 0.010, exact). However, post hoc pairwise comparisons (Tukey on ranks) did not reveal any statistically significant differences between specific group pairs.

Evaluation of XOR Activity: The oxidative brain damage model used in our experiments closely resembles the pathological stage observed in clinical stroke. One of the key pro-oxidative enzymes involved in this process is xanthine oxidoreductase (XOR; EC 1.17.3.2), which can be activated in macrophages localized within damaged brain regions [26, 27]. To investigate the potential molecular mechanism of PRP-1 nanoparticles, we evaluated their effect on XOR activity in vitro.

XOR was purified from milk, and its activity was detected in the 17th–18th fractions during the gel filtration stage (Figure 5A), consistent with its high molecular weight and late elution. Following semi-affinity purification via ion-exchange chromatography, the

protein's purity was assessed using RP-HPLC (Figure 5B). Two different concentrations of purified XOR were analyzed by RP-HPLC (0.018 mg/mL and 0.088 mg/mL).

Figure 5C presents the inhibitory effect of PRP-1 on XOR activity. Four experimental groups were tested: control (0.19 ± 3.23 × 10^{-3} ug/g of tissue per minute), enzyme with substrate (0.40 ± 1.62 × 10^{-3} ug/g of tissue per minute), enzyme with the well-known inhibitor - allopurinol (0.20 ± 8.70 × 10^{-4} u ug/g of tissue per minute g/ml) and enzyme in the presence of PRP-1 (0,1 ug/1 ml) (0.14 ± 3.35 × 10^{-3} ug/g of tissue per minute). In comparison with control, PRP-1 reduced XOR activity by approximately 65%, whereas allopurinol inhibited activity by about 50% under the same conditions. At higher PRP-1 concentrations (0,4 µgµgµLsuppressedµg/1 mL of reaction mixture), XOR activity was completely suppressed, indicating a potent, dose-dependent inhibition comparable to or superior to that of allopurinol.

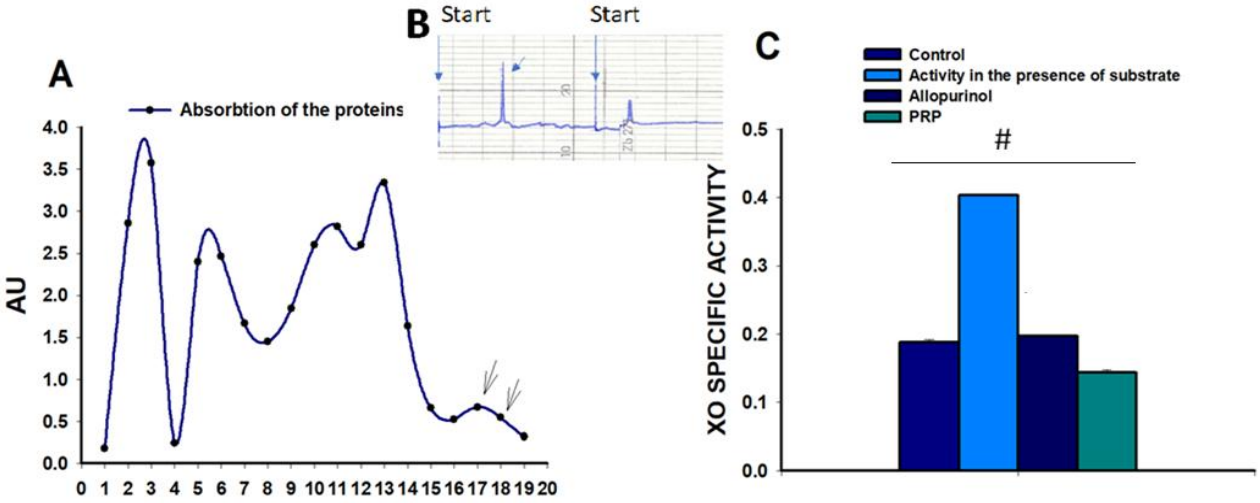

Figure 5. Purification of XOR and evaluation of enzyme activity in the presence of PRP-1. A. Gel filtration of the proteins. The arrows to to the fractions, pointing to the fractions where XOR activity was detected. B. Final evaluation of XOR purity. Two different concentrations of the enzyme are presented in the pictures (0,018 mg/ml and 0,088 mg/ml). C. Evaluation of XOR activity in the presence/absence of PRP-1 (n=5). Because the assumption of equal variances was violated, a Kruskal–Wallis test was used. The overall test indicated a statistically significant difference among the four groups, H(3) = 6.667, p = 0.010 (exact). However, post hoc pairwise comparisons (Tukey on ranks) did not reveal any statistically significant differences between specific group pairs.

The horizontal bar the ANOVA test application, indicating that all groups are compared simultaneously.

Circulation of Particles under Normal and Experimental Brain Damage Conditions: Particle circulation in all groups, under both normal and pathological conditions, was analyzed using Evans Blue (EB). Blood samples were collected daily from the tail vein for analysis. Samples were centrifuged at 3,000 × g, and the supernatant was stained with EB to visualize remaining particles. Particle counts were determined using a Boeco trinocular microscope (Germany).

The number of particles was normalized to a standard blood volume for animals weighing 200–250 g, accounting for each animal's hematocrit level. Figure 6A illustrates the circulation of NPs and NP/PRP-1 under both normal and pathological conditions. A significant difference in particle circulation under stroke conditions was observed on day 3, with values of 20.0% ± 5.0% for NPs and 31.0% ± 4.0% for NP/PRP-1.

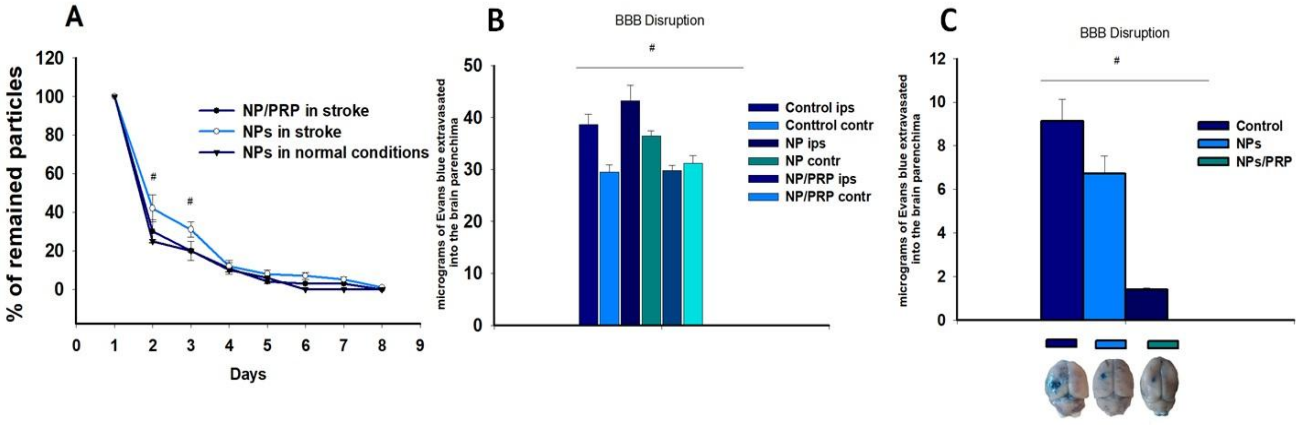

Figure 6. In vivo behavior of the NPs. A. Circulation of the particles in physiological and pathological conditions. The results are presented as the remaining percentiles. The absolute number of particles was calculated by the light microscopy (Boeco, Germany) after staining them with Evans Blue.

Two-way repeated measures ANOVA showed a significant main effect of time, $F(7, 7) = 1196.32$, $p < 0.001$, and a significant interaction between group and time, $F(7, 7) = 7.22$, $p = 0.009$. Post hoc Holm-Sidak tests indicated that the experimental group retained significantly more particles than the control group at 2 h ($p < 0.001$), 3 h ($p = 0.001$), and 6 h ($p = 0.031$), (n=5 per group). No significant group differences were observed at other time points.

The absolute amount of the EB, extracted from the ipsilateral vs contralateral hemispheres of the brain tissue for three groups: naïve animals, injected with albumin NPs, and albumin/PRP-1 NPs. The amount of dye was measured using a Cary 60 (Agilent, USA) at 620 nm. A Way ANOVA test was used, and the results were statistically significant, with # p<0.05 (n=5 per group). C.

The absolute amount of the EB, extracted from brain tissue for three groups as the difference between ipsilateral vs contralateral hemispheres. Groups: naïve animals, injected with albumin NPs and albumin/PRP-1 NPs. At the bottom of the graphs the representative pictures of the entire brain pictures of the groups are presented. A Way ANOVA test was used, and the results were statistically significant, with #p<0.05 (n=5 per group).

The horizontal bar is the sign of the ANOVA test application, indicating that all groups are compared simultaneously.

The Coupling of PRP-1 with NPs Protects Against BBB Disruption: We examined blood–brain barrier (BBB) disruption following experimental stroke. One hour after administering 1 mL of 4% Evans Blue (EB), animals were perfused with saline and subsequently decapitated. Brains were frozen and sectioned into 1 mm coronal slices. EB was extracted, and its concentration was measured spectrophotometrically, as described in the Methods section.

The most significant difference in EB accumulation was observed in the control group between ipsilateral and contralateral hemispheres (38.6 ± 2.03 vs. 29.48 ± 1.41, Figure 6). In animals injected with NPs, the hemispheric difference was more pronounced compared to the NP/PRP-1 group (43.19 ± 3.08 vs. 36.46 ± 1.0 for NPs compared to 29.76 ± 1.14 vs. 31.17 ± 1.53, $p < 0.05$, One-Way ANOVA).

DISCUSSION

Biological carriers are preferred over chemical prototypes for drug delivery due to their superior safety and efficiency. In our study on experimental stroke, albumin particles were selected as biological carriers. Both literature data and our experiments support the effectiveness of albumin treatment in this context [18].

Albumin helps retain water in the bloodstream, reducing brain edema caused by BBB disruption and ischemic processes. However, a recent clinical trial failed to demonstrate the efficacy of albumin in stroke patients, likely due to suboptimal dosing or timing of treatment [28].

Based on the ALIAS (Albumin in Acute Ischemic Stroke) trials' results, the treatment with intravenous albumin 25% at 2 g/kg did not improve outcome at 90 days and was associated with increased rates of intracerebral hemorrhage and pulmonary edema [28]. A high dose of albumin can significantly alter the oncotic pressure of the blood and lead to the development of hemorrhage and pulmonary edema.

Excessive infusion of hyperoncotic (20–25%) albumin can cause fluid shifts into the vascular space, increasing cardiac preload and precipitating pulmonary edema, especially in patients with heart failure or increased capillary permeability (e.g., sepsis, ARDS) [29]. Additionally, hyperoncotic albumin can increase intravascular shear stress and capillary wall tension, leading to microhemorrhages in fragile vascular networks (lungs, brain) [30].

In contrast to free albumin, albumin NPs exhibit significantly lower oncotic pressure than free albumin because aggregation and crosslinking reduce the number of osmotically active molecules and prevent their diffusion across semipermeable membranes [31]. Thus, prepared and suggested, as the drug carriers, albumin particles are clinically safer than free albumin molecules in the bloodstream.

From the other hand by binding the PRP-1 with the albumin particles, we were able to prolong the circulation time of the peptide as well as to increase the efficiency (low dosage utility as well as economic potential medicines).

Other groups' experimental findings also suggest that PRP-1 has neuroprotective properties, as demonstrated in models of Alzheimer's disease [32] and Parkinson's disease (unpublished results). Based on other investigations, in vitro, PRP-1 protects cortical and hippocampal cell cultures from apoptosis induced by staurosporine [1-2] and exhibits antioxidant properties [26-27].

Thus, to enhance therapeutic effects, we developed a dual-treatment approach combining albumin NPs with PRP-1. Albumin particles maintain blood volume and facilitate delivery, while PRP-1 conjugation enhances neuroprotection and reflects antioxidant abilities.

Additionally, we have demonstrated that PRP-1 alone inhibited protease activity but was more effective when combined with general inhibitors such as potassium sodium tartrate ($KNaC_4H_4O_6{\cdot}4H_2O$). Interestingly, based on the other laboratories' data, proline-rich peptides (PRPs) can inhibit microbial proteases at high concentrations [33]. We suggest that the presented broad protease inhibiting activity of PRP-1 might explain its ability to protect the BBB from matrix metalloproteases, which are "key players" in BBB disruption after stroke [34].

Several factors influence nanoparticle efficacy as drug carriers. Particle size affects biodistribution, cellular uptake, and clearance. Smaller carriers (<200 nm) provide lower drug-loading capacity but enhance circulation time and tissue penetration. Particle shape influences uptake and stability, while rigidity or flexibility affects tissue penetration [35].

TEM analysis revealed particle sizes before sedimentation and filtration (Figure 1). Refinement via

filtration produced particles ~160 nm in diameter. Zeta potential measurements, which assess stability, showed no significant differences between albumin NPs and albumin/PRP-1 carriers. Conductivity was slightly but significantly higher in PRP-1/NPs, potentially due to proline binding Li^+ ions [36].

This effect was not observed in electrophoretic mobility experiments, likely due to experimental limitations. Thus, we were able to create small size and stable PRP-1/NPs. Circulation studies demonstrated that PRP-1-conjugated NPs remained in the bloodstream longer.

One key mechanism in stroke development involves the generation of reactive oxygen species (ROS), which initiate lipid peroxidation of neuronal and endothelial cell membranes. During ischemia and especially upon reperfusion, excess ROS, such as hydroxyl radicals, react with polyunsaturated fatty acids in the lipid bilayer, forming lipid radicals and hydroperoxides that compromise membrane integrity and increase permeability of the BBB. This damage propagates a chain reaction, ultimately disrupting cell and microvascular structure, contributing to infarct progression and cerebral edema [37].

Taking into consideration that previous studies have shown PRP-1 to possess potent antioxidant properties [38] and XOR inhibition studies proved the other data, we selected a model [17] that would allow us to clarify the antioxidant effects of PRP-1 in the setting of experimental stroke.

Neurological deficit assessments were inconclusive, likely due to localization. Three mm in diameter damage localized in temporal cortex hasn't induced detectable neurological deficit, which is in agreement with the data obtained from the other laboratories [39-40].

In fluid impact models of traumatic brain injury, the mild traumatic lesion was localized in the right lateral parietal cortex. The lesion had no effects on general neurological function, motor activity (activity boxes, rota-rod and paw reaching tests), habituation to a novel environment (holeboard), spatial learning ability (Morris water maze) or anxiety (elevated plus-maze) [39].

The other group of investigators demonstrated that rats with unilateral MFC (Medial Frontal Cortex) lesions show a vivid change in decision-making on an effort-based decision-making task and absent of the neurological deficit. Also, rats with unilateral dopaminergic midbrain lesions, based on obtained results, did exhibit a motoric turning bias, but were unimpaired on the effort-based decision-making task [40]. Consequently, the small unilateral lesions in temporal cortex are not mostly detectable – "silent" zones and plasticity and compensation (contralateral cortex, subcortical circuits) frequently can mask deficits over days–weeks [41].

The absence of a comprehensive battery of neurological test results, possibly due to insufficient sensitivity, is one of the study's limitations. Further development and application of behavioral tests are needed to more precisely evaluate the impact of the newly developed formulations.

In accordance with the results obtained by our lab, PRP-1 strongly binds to XOR and inhibits its activity, highlighting its antioxidant potential. In silico and in vitro results were approved in vivo experiments. In the final study phase, oxidative stress was induced by intracranial injection of hydrogen peroxide, and animals were monitored for 7 days. A single treatment of PRP-1, NPs, or PRP-1/NPs was administered based on circulation data. PRP-1/NPs most effectively preserved BBB integrity under experimental stroke conditions.

Our study demonstrates that conjugation of PRP-1 to albumin nanoparticles prolongs peptide stability and partially preserves BBB integrity in an oxidative brain-injury model.

PRP/albumin NPs were injected intravenously via the jugular vein as the therapeutic compounds.

Encapsulation technology can stand as a key opportunity for bioactive peptides by improving their solubility, sensory properties, and stability. However, further research is needed to clarify how encapsulation influences peptide bioavailability and interactions with food, because efficient intestinal absorption is essential for physiological efficacy. Limited studies, such as that by Cian et al. [42], showed that microencapsulated Phaseolus lunatus peptides enhanced enzyme inhibitory activity after simulated digestion, suggesting that bioaccessibility is improved.

Some proteins have been to a lesser extent used as encapsulating materials for bioactive peptides, despite the fact that they possess advantages such as nutritional value and good emulsifying and gelling properties. Their chemical similarity with peptides may enhance interactions and structural stability [43]. For instance, whey protein isolate enhanced hydrophobic interactions during riboflavin encapsulation, while alginate/whey protein microcapsules containing collagen peptides protected riboflavin in gastric fluid but allowed degradation in intestinal fluid [44].

Additionally, within the capsules, peptides can serve as the preserving agents, because of the antimicrobial and antioxidant properties [45].

As a stroke preventive bioactive compound, PRP /albumin NPs can be used orally, as the food-compatible delivery systems (e.g., fortified dairy or beverage matrices, encapsulated nutraceuticals) where nanoparticle encapsulation addresses both stability during digestion and targeted bioavailability.

Such an approach opens opportunities for preventative or adjunctive dietary strategies to reduce stroke risk and support neuroprotection, provided subsequent gastrointestinal stability, safety and bioavailability in humans, improving public health [46-50].

Study Limitations: One limitation of the study is the absence of a comprehensive set of neurological test results, possibly due to the limited sensitivity of the applied methods or the location of the small sized damage in the “silent” area of the temporal cortex. Further development and implementation of behavioral assessments are required to evaluate the effects of the newly developed formulations accurately.

Another limitation of the study is the lack of *in vivo* evaluation of XOR activity in the experimental model of brain oxidative damage, with and without the administered formulations.

Overall, PRP-1-conjugated albumin nanoparticles represent a promising therapeutic candidate for experimental oxidative brain injury. This combined approach leverages the complementary properties of albumin and PRP-1, offering a novel, potentially more effective strategy to protect the BBB and mitigate stroke-related damage.

CONCLUSION

PRP-1 demonstrates consistent neuroprotective and antioxidant properties across various experimental models, including Alzheimer’s disease and neuronal apoptosis.

To improve therapeutic outcomes, we, for the first time, based on our knowledge, developed a dual-delivery system coupling PRP-1 with albumin NPs. This strategy provides synergistic benefits: albumin prolongs circulation and enhances delivery, while PRP-1 confers neuroprotection and reduces peptide degradation.

Characterization studies confirmed that PRP-1/albumin NPs are stable, with a favorable size (~160 nm)

and circulation properties. In the oxidative stress stroke model induced by hydrogen peroxide, PRP-1/albumin NPs preserved BBB integrity more effectively than albumin NPs alone. PRP-1's ability to inhibit XOR further supports its antioxidant role.

Thus, for the first time we have clarified one of the possible mechanisms of PRP-1 anti-oxidative properties, which is the inhibition of XOR activity and prevention of the formation of free radicals.

Moreover, due to the long circulation abilities, PRP-1/albumin NPs might replace the multiple injection treatment strategy, making the formulation more economically beneficial.

In addition, we suggest that PRP/albumin NP encapsulation might stabilize the formulation in the gastrointestinal tract and improve bioavailability, making the formulation a promising bioactive compound.

Given PRP-1's antioxidant properties, the newly developed formulation may serve as a carrier for other nutrients and exhibit matter-preserving properties.

List of abbreviations used: CVDs (cardiovascular diseases); PRP-1 (Proline Rich Peptide); TEM (Transmission Electron Microscopy); BBB (Blood Brain Barrier); NP(s) (Nanopartciles); XOR (Xanthin Oxidoreductase); RP-HPLC (Reverse-Phase High Performance Liquide Chromatography); GA (Glutaraldehyde); I.P. (Intraperitoneal); ANOVA (One-way analysis of variance); EB (Evans Blue);

Authors' contributions: KED: organizing, planning, partially performing experiments, writing the paper, editing, and submitting; NZ: performing experiments, helping in the writing of "Methods" part**;** RK: performing experiments, helping in the writing of Docking analyses part**;** MK: performing experiments, helping in the writing of XOR purification and activity measurement part in "Methods" section; KT: performing experiments, helping in the writing of XOR purification and activity measurement part in "Methods" section**;** AT: performing experiments, helping in the writing of DLS analyses measurement part in "Methods" section; AM: performing experiments, helping in the writing of "Methods" part; MAY: organizing paper, editing, planning the experiments; SGC: organizing paper, editing, planning the experiments.

Competing interests: The authors have no relevant financial or non-financial interests to disclose.

Acknowledgments: We thank Gor Chailyan for synthesizing and providing PRP-1 for the experiments.

Funding statement: The work was performed based on the Scientific and Technical Contractual (Thematic) Activity-related grant from State Budget Funding – 2021-2024.

REFERENCES

1. Galoyan AA. Brain neurosecretory cytokines: immune response and neuronal survival. 2004. DOI: https://doi.org/10.1007/978-1-4419-8893-5
2. Galoyan AA, Krieglstein J, Klumpp S, Danielyan KE, Galoian KA, Kremers W, et al. Effect of hypothalamic proline-rich peptide (PRP-1) on neuronal and bone marrow cell apoptosis. *Neurochem Res.* 2007;32(11):1898-1905. DOI: https://doi.org/10.1007/s11064-007-9379-9
3. Carlson DM. Salivary proline-rich proteins: biochemistry, molecular biology, and regulation of expression. *Crit Rev Oral Biol Med.* 1993;4(3-4):495-502. DOI: https://doi.org/10.1177/10454411930040033401
4. Gladkevich A, Bosker, F., Korf, J., Yenkoyan K, Vahradyan H, Aghajanov M. Proline-rich polypeptides in Alzheimer's disease and neurodegenerative disorders - Therapeutic potential or a mirage? *Progress in Neuro-Psychopharmacology & Biological Psychiatry*. 2007;31:1347-1355. DOI: https://doi.org/10.1016/j.pnpbp.2007.06.005
5. Knaryan VH, Samantaray S, Varghese M, Srinivasan A, Galoyan AA, Mohanakumar KP. Synthetic bovine proline-rich-polypeptides generate hydroxyl radicals and fail to

protect dopaminergic neurons against 1-methyl-4-phenyl-1,2,3,6-tetrahydropyridine-induced dopaminergic neurotoxicity in mice. *Neuropeptides.* 2006;40(4):291-298. DOI: https://doi.org/10.1016/j.npep.2006.03.005

6. Böttger R, Hoffmann R, Knappe D. Differential stability of therapeutic peptides with different proteolytic cleavage sites in blood, plasma and serum. *PLoS One.* 2017;12(6): e0178943. DOI: https://doi.org/10.1371/journal.pone.0178943
7. Eger BT, Okamoto K, Enroth C, Sato M, Nishino T, Pai EF and Nishino T. Purification, crystallization, and preliminary X-ray diffraction studies of xanthine dehydrogenase and xanthine oxidase isolated from bovine milk. *Acta Crystallogr D Biol Crystallogr*. 2000;56: 1656-8. DOI: https://doi.org/10.1107/s0907444900012890
8. Ozer N, Müftüoglu M, Ataman D, Ercan A, Ögüs IH. Simple, high-yield purification of xanthine oxidase from bovine milk. *J Biochem Biophys Methods.* 1999;39:153-159. DOI: https://doi.org/10.1016/s0165-022x(99)00012-3
9. Litwack G, Bothwell JW, Williams JN, Jr., Elvehjem CA. A colorimetric assay for xanthine oxidase in rat liver homogenates. *J Biol Chem. 1953*;200:303-310. DOI: https://pubmed.ncbi.nlm.nih.gov/13034787
10. Aganyants HA, Nikohosyan G, Danielyan KE. Albumin microparticles are the carriers for allopurinol are applicable for the treatment of ischemic stroke. *International Nano Letters.* 2016;6:35–40. DOI: https://doi.org/10.1007/s40089-015-0169-0
11. Galoyan AA, Sarkissian JS, Chavushyan VA, Meliksetyan Irina B., Avagyan Zaruhi E., Poghosyan, Mikhail V. et al. Neuroprotection by hypothalamic peptide proline-rich peptide-1 in Abeta25-35 model of Alzheimer's disease. *Alzheimer's Dement.* 2008;4:332-344. DOI: https://doi.org/10.1016/j.jalz.2007.10.019
12. Ohanyan N, Abelyan N, Manukyan A, Hayrapetyan V, Chailyan S, Tiratsuyan S, et al. Tannin-albumin particles as stable carriers of medicines. *Nanomedicine (London, England).* 2024;19:689–708. DOI: https://doi.org/10.2217/nnm-2023-0275
13. Khoshnejad M, Shuvaev VV, Pulsipher KW, Dai C, Hood ED,Arguiri E,et al. Vascular accessibility of endothelial targeted ferritin nanoparticles. Bioconjug Chem. 2016;27(3):628-37. DOI: https://doi.org/10.1021/acs.bioconjchem.5b00641
14. Roughan JV, Flecknell PA. Effects of surgery and analgesic administration on spontaneous behaviour in singly housed rats. Res Vet Sci. 2000;69(3):283-8. DOI: https://doi.org/10.1053/rvsc.2000.0430
15. Carpenter JW, Marion CJ. Exotic Animal Formulary. 5th ed. St. Louis (MO): Elsevier; 2019. https://pmc.ncbi.nlm.nih.gov/articles/PMC6294031/. Retrieved on 11.27.25
16. Paxinos G, Watson C. The rat Brain in stereotaxic coordinates, 7th ed. San Diego, CA, USA: Academic Press (Elsevier), 2013.
17. Danielyan KE, Simonyan AA. Protective abilities of pyridoxine in experimental oxidative stress settings in vivo and in vitro. *Biomed Pharmacother*. 2017;86:537-540. DOI: https://doi.org/10.1016/j.biopha.2016.12.053
18. Belayev L, Saul I, Busto R, et al. Albumin treatment reduces neurological deficit and protects blood-brain barrier integrity after acute intracortical hematoma in the rat. *Stroke.* 2005;36(2):326-331. DOI: https://doi.org/10.1161/01.STR.0000152949.31366.3d
19. Bederson JB, Pitts LH, Tsuji M, Nishimura MC , Davis RL, and Bartkowski H. Rat middle cerebral artery occlusion: evaluation of the model and development of a neurologic examination. *Stroke.* 1986;17:472-476. DOI: https://doi.org/10.1161/01.str.17.3.472
20. De Ryck M, Van Reempts J, Borgers M, Wauquier A, and Janssen P A . Photochemical stroke model: flunarizine prevents sensorimotor deficits after neocortical infarcts in rats. *Stroke.* 1989;20:1383-1390. DOI: https://doi.org/10.1161/01.STR.20.10.1383
21. Belayev L, Busto R, Ikeda M, Lee L R, Kajiwara A, Morgan L, et al. Protection against blood-brain barrier disruption in focal cerebral ischemia by the type IV phosphodiesterase inhibitor BBB022: a quantitative study. *Brain Res.* 1998; 787(2):277-285. DOI: https://doi.org/10.1016/s0006-8993(97)01499-6
22. Hille R, Nishino T. Flavoprotein structure and mechanism. Xanthine oxidase and xanthine dehydrogenase. *FASEB J.* 1995;9:995–1003. DOI: https://pubmed.ncbi.nlm.nih.gov/7649415/
23. Kobayashi K, Miki M, Okamoto K. Electron transfer process in milk xanthine dehydrogenase as studied by pulse radiolysis. *J Biol Chem.* 1993;268:24642–24646. DOI: https://pubmed.ncbi.nlm.nih.gov/8227023/
24. Nishino T, Okamoto K, Eger BT, Pai EF, Nishinoet T. Mammalian xanthine oxidoreductase - mechanism of transition from xanthine dehydrogenase to xanthine oxidase. *FEBS J.* 2008;275:3278-3289.

DOI: https://doi.org/10.1111/j.1742-4658.2008.06489.x

25. Kanda M, Brady FO, Rajagopalan KV, Handler P. Studies on the dissociation of flavin adenine dinucleotide from metalloflavoproteins *J Biol Chem.* 1972;247:765–70.
DOI: https://pubmed.ncbi.nlm.nih.gov/4333512/
26. Davtyan TK, Manukyan HM, Hakopyan GS, Nana R. Mkrtchyan, . Avetisyan SA & Galoyan AA. Hypothalamic proline-rich polypeptide is an oxidative burst regulator. *Neurochem Res.* 2005;30(3):297-309. DOI: https://doi.org/10.1007/s11064-005-2603-6
27. Davtyan K, Manukyan HA, Mkrtchyan R, Avetisyan SA & Galoyan AA. Hypothalamic proline-rich polypeptide is a regulator of oxidative burst in human neutrophils and monocytes. *Neuroimmunomodulation.* 2005;12(5):270-84. DOI: https://doi.org/10.1159/000087105
28. Martin RH, Yeatts SD, Hill MD, Moy CS, Ginsberg MD, and Palesch YY. ALIAS (Albumin in Acute Ischemic Stroke) trials: Analysis of the combined data from parts 1 and 2. *Stroke.* 2016;47(9):2355-2359. DOI: https://doi.org/10.1161/STROKEAHA.116.012825
29. Wiedermann CJ, Joannidis M. Albumin replacement in severe sepsis or septic shock. *N Engl J Med*. 2014;371:83. DOI: https://doi.org/10.1056/NEJMc1405675
30. Vincent JL, Navickis RJ, Wilkes MM. Morbidity in hospitalized patients receiving human albumin: a meta-analysis of randomized, controlled trials. *Crit Care Med.* 2004;32:2029-2038. DOI:https://doi.org/10.1097/01.ccm.0000142574.00425.e9
31. Hall JE, Hall ME. Guyton and Hall Textbook of Medical Physiology. 14th ed. Elsevier, 2020. DOI: http://evolve.elsevier.com/Hall/physiology/
32. Yenkoyan K, Safaryan K, Chavushyan V, Meliksetyan I, Navasardyan G, Sarkissian J, et all. Neuroprotective action of proline-rich polypeptide-1 in β-amyloid induced neurodegeneration in rats. *Brain Res Bull*. 2011;86(3-4):262-271. DOI: https://doi.org/10.1016/j.brainresbull.2011.08.003
33. Couto MA, Harwig SS, Lehrer RI. Selective inhibition of microbial serine proteases by eNAP-2, an antimicrobial peptide from equine neutrophils. *Infect Immun.* 1993;61(7): DOI: https://doi.org/10.1128/iai.61.7.2991-2994.1993
34. Shi T, Yue S, Xie C, Li X, Yang D, Hu L, et all. MMP-2-mediated Scube2 degradation promotes blood-brain barrier disruption by blocking the interaction between astrocytes and endothelial cells via inhibiting Sonic hedgehog pathway during early cerebral ischemia. *J Neurochem.* 2024;168:1877-1894. DOI: https://doi.org/10.1111/jnc.16021
35. Agrahari V, Burnouf PA, Burnouf T, Agrahari V. Nanoformulation properties, characterization, and behavior in complex biological matrices: challenges and opportunities for brain-targeted drug delivery applications and enhanced translational potential. *Adv Drug Deliv Rev.* 2019;148:146–180. DOI: https://doi.org/10.1016/j.addr.2019.02.008
36. Khalili B. An insight into the interaction of L-proline with the transition metal cations Fe(2+), Co(2+), Ni(2+): a gas phase theoretical study. *J Mol Model.* 2016;22. DOI: https://doi.org/10.1007/s00894-015-2865-0
37. Zheng Y, Tan X, Wang X, Mao R, Guo J. Targeting ferroptosis with natural products in stroke: therapeutic mechanisms and translational opportunities. *Front Pharmacol.* 2025;16:1586345. DOI: https://doi.org/10.3389/fphar.2025.1586345
38. Tavadyan LA, Galoian KA, Harutunyan LA, Tonikyan H. G. & Galoyan A. A. Antioxidant and electron donating function of hypothalamic polypeptides: galarmin and Gx-NH2. *Neurochem Res.* 2010;35:947-52. DOI: https://doi.org/10.1007/s11064-010-0173-8
39. Hogg S, Moser PC, Sanger DJ. Mild traumatic lesion of the right parietal cortex of the rat: selective behavioural deficits in the absence of neurological impairment. *Behav Brain Res.* 1998;93:143-155. DOI: https://doi.org/10.1016/s0166-4328(97)00146-0
40. Croxson PL, Walton ME, Boorman ED, Rushworth MFS., Bannerman DM.. Unilateral medial frontal cortex lesions cause a cognitive decision-making deficit in rats. *Eur J Neurosci.* 2014;40:3757-3765. DOI: https://doi.org/10.1111/ejn.12751
41. Jones TA, Chu CJ, Grande LA, Gregory AD. Motor skills training enhances lesion-induced structural plasticity in the motor cortex of adult rats. *The Journal of Neuroscience.* 1999;19: 10153-10163. DOI:https://doi.org/10.1523/JNEUROSCI.19-22-10153.1999
42. Cian RE, Campos-Soldini A, Chel-Guerrero L, Drago SR, Betancur-Ancona D. Effect of simulated gastrointestinal digestion on the inhibitory properties of microencapsulated Phaseolus lunatus peptides. *Int J Food Sci Technol.* 2019;54:2002–2009. DOI: https://doi.org/10.1111/ijfs.14031

43. Mohan A, Rajendran SRCK, He QS, Bazinet L, Udenigwe CC. Encapsulation of food protein hydrolysates and peptide fractions: A review. *RSC Adv.* 2015;5:79270–79278. DOI: https://doi.org/10.1039/C5RA13419F
44. Lajmi K, Gómez-Estaca J, Hammami M, Martínez-Alvarez O. Encapsulation of bioactive peptides: A strategy to improve stability and bioavailability. *Food Biosci.* 2019;28:99–108. DOI: https://doi.org/10.1016/j.fbio.2019.01.014
45. Aguilar-Toalá JE, Quintanar-Guerrero D, Liceaga AM, Zambrano-Zaragoza ML. Encapsulation of bioactive peptides: a strategy to improve the stability, protect the nutraceutical bioactivity and support their food applications. *RSC Adv*. 2022;12:6449-6458. DOI: https://doi.org/10.1039/d1ra08590e
46. McClements DJ. Encapsulation, protection, and delivery of bioactive proteins and peptides using nanoparticle and microparticle systems: A review. *Adv Colloid Interface Sci.* 2018;253:1-22. DOI: https://doi.org/10.1016/j.cis.2018.02.002
47. Rezagholizade-Shirvan A, Soltani M, Shokri S, Radfar R, Arab M, Shamloo E. Bioactive compound encapsulation: Characteristics, applications in food systems, and implications for human health. *Food Chem X.* 2024;24:101953. DOI: https://doi.org/10.1016/j.fochx.2024.101953
48. Janigashvili G, Shekiladze E, Chkhikvishvili I, Enukidze M, Machavariani M, Ratiani L, et all. Effect of liposomal complexes of quercetin-rich flavonoids from French Marigold (Tagetes patula L.) on Jurkat cell viability. *Bioactive Compounds in Health and Disease.* 2024;7(3):131-144. DOI: https://doi.org/10.31989/bchd.v7i3.1293
49. Martirosyan DM, Stratton S. Advancing functional food regulation. *Bioactive Compounds in Health and Disease.* 2023;6(7):166–171. DOI: https://doi.org/10.31989/bchd.v6i7.1178
50. Keawyok K, Jodnak S. Development of high protein supplements containing synbiotics for athletes. *Bioactive Compounds in Health and Disease.* 2025;8(2):56–75. DOI: https://doi.org/10.31989/bchd.8i2.1540